

Epitaxially strained SnTiO_3 at finite temperatures ^{*}

Dawei Wang^{a)†}, Laijun Liu^{b)‡}, Jia Liu^{c)}, Nan Zhang^{d)}, Xiaoyong Wei^{d)}

^{a)}School of Microelectronics and State Key Laboratory for Mechanical Behaviour of Materials,
Xi'an Jiaotong University, Xi'an 710049, China

^{b)}College of Materials Science and Engineering,
Guilin University of Technology, Guilin 541004, China

^{c)}State Key Laboratory for Mechanical Behavior of Materials &
School of Materials Science and Engineering, Xi'an Jiaotong University, Xi'an 710049, China

^{d)}Electronic Materials Research Laboratory-Key Laboratory of the Ministry of Education and
International Centre for Dielectric Research, Xi'an Jiaotong University, Xi'an 710049, China

June 3, 2022

Abstract

Combining the effective Hamiltonian approach and direct *ab initio* computation, we obtain the phase diagram of SnTiO_3 with respect to epitaxial strain and temperature, demonstrating the complex features of the phase diagram and providing insight into this system, a presumably simple perovskite. Two triple points, as shown in the phase diagram, may be exploited to achieve high-performance piezoelectric effects. Despite the inclusion of the degree of freedoms related to oxygen octahedron tilting, the ferroelectric displacements dominate the structural phases over the whole misfit strain range. Finally, we show SnTiO_3 can change from hard to soft ferroelectrics with the epitaxial strain.

Keywords: SnTiO_3 , phase diagram, epitaxial strain

PACS: 77.80.-e, 77.84.-s, 81.30.Bx

1. Introduction

Piezoelectricity is a phenomenon in certain materials that strain and electric polarization can induce and/or influence each other. Ferroelectric materials, which are inherently piezoelectric, can produce an electric polarization proportional to the load, in response to an applied mechanical strain. Similarly, such materials will produce a mechanical deformation (strain) in response to an applied voltage. Switchable polarization makes

^{*}Project supported by the National Natural Science Foundation of China (Grant No. 11574246, 51390472, U1537210, and 11564010), the National Basic Research Program of China (Grant No. 2015CB654903), the Natural Science Foundation of Guangxi (GA139008), and the "111" Project (Grant No. B14040).

[†]Corresponding author. E-mail:dawei.wang@mail.xjtu.edu.edu

[‡]Corresponding author. E-mail:2009011@glut.edu.edu

ferroelectrics a critical component in memories, actuators, electro-optic devices, and potential candidates for nanoelectronics [1].

In recent years, it has been found that materials of high-performance piezoelectricity are often associated with morphotropic phase boundary (MPB), with examples including $\text{Pb}(\text{Zr},\text{Ti})\text{O}_3$ [2] and $(\text{K},\text{Na})\text{NbO}_3\text{-LiTaO}_3\text{-LiSbO}_3$ [3], or triple points, e.g. in $(\text{Ba},\text{Ca})(\text{Zr},\text{Ti})\text{O}_3$ [4]. Engineering solid solutions to a certain composition can create phase boundaries and tricritical points, where the crystal structure changes abruptly, inducing maximal piezoelectric properties. Three important situations have been extensively studied: (i) MPB in pure perovskites that separates regions of the tetragonal from the rhombohedral symmetry [5]; (ii) MPB formed in perovskites dissolved with a small amount of non-perovskite-structured materials that can cause lattice distortions [3] and grain boundary effects [6]; (iii) Regions close to a triple point where cubic paraelectric phase (C), ferroelectric rhombohedral (R), and tetragonal (T) phases meet [4]. In addition to MPB, epitaxial thin-film growth, which introduces intrinsic lattice strain, has matured as another important method to design desired ferroelectric materials, important for highly integrated design and intelligent control technology [7,8]. Strain engineering, widely adopted, can tune the large $2p\text{-}3d$ charge hybridisation between the strongly correlated $3d$ electrons in transition metal ions and the $2p$ electrons of oxygens [9–12]. For instance, both compressive and tensile strains increase the Ni $3d$ band width and favour the metallic phase in NdNiO_3 [13]. In addition, substrate clamping will force the temperature dependence of in-plane lattice constants of the grown films to follow that of the substrates, which may lead to unexpected phase transitions and domain formation [14,15]. Therefore, strain constraint can even introduce multi-phase coexistence in thin films, which makes it an attractive method to fine tuning properties of films.

Nowadays commonly used high-performance piezoelectric materials, including PbTiO_3 and $\text{Pb}(\text{Mn},\text{Nb})\text{O}_3$, contain hazardous lead (Pb). Since Pb is harmful to environment and human health, lead-free ferroelectric materials are highly desired. Many lead-free materials are based on $(\text{Bi}_{0.5},\text{Na}_{0.5})\text{TiO}_3$, $(\text{K},\text{Na})\text{NbO}_3$ or BaTiO_3 , however, their performance is still sub-optimal compared to Pb-containing materials [16]. Since Sn and Pb belong to the same family, SnTiO_3 is expected to achieve high-performance piezoelectricity with environmentally benign elements [17]. Indeed, SnTiO_3 has large polarization and large axial ratio [18,19], even larger than PbTiO_3 , making it a promising candidate. But for various reasons, SnTiO_3 bulk material is hard to prepare, since Sn^{2+} can easily become Sn^{4+} , and Sn is prone to enter into the B site (where the Ti ion stays) due to its small ionic radius. However, researchers continued to look for opportunities to exploit the remarkable properties of SnTiO_3 . For instance, researchers have considered Sn-doped BaTiO_3 [20,21], Bennett *et al* considered $\text{Sn}(\text{Al}_{0.5},\text{Nb}_{0.5})\text{O}_3$ [22], while Suzuki *et al* obtained Sn-doped SrTiO_3 [23], and Laurita investigated $(\text{Sr},\text{Sn})\text{TiO}_3$ and $(\text{Ba},\text{Ca},\text{Sn})\text{TiO}_3$ [24]. Recently, Agarwal *et al* [25] obtained perovskite phase SnTiO_3 with the atomic-layer deposition technique. This is an important breakthrough that will excite more work on SnTiO_3 .

In addition to experimental work, there are also many theoretical investigations on SnTiO_3 [17,19,26–30]. However, most of previous theoretical investigations are based on direct *ab initio* computation, which cannot provide information regarding SnTiO_3 at finite temperatures. Therefore, important questions remain unanswered. For instance, what are the conditions for the existence of different ferroelectric phases? How is the phase diagram of SnTiO_3 like? Can such a seemingly simple perovskite (SnTiO_3 is not solid solution and no doping is applied) possess complex features? In this work, we will focus on the finite temperature properties

of epitaxially strained SnTiO_3 and address these questions. We note that such information will be useful for the fabrication of SnTiO_3 bulk, or the growth of SnTiO_3 film, and engineering SnTiO_3 -containing ferroelectric materials. Since SnTiO_3 bulk is not available, there is not much *a priori* information at finite temperatures that can be used in this work. While our computational results are less convincing without the support from experiments, it demonstrates the value of theoretical and numerical work, i.e., their power to predict something unknown – this is one of the reasons that motivated this investigation.

2. Method

To fully understand SnTiO_3 , knowing all its possible phases under various conditions is desired. However, it is not trivial to achieve this goal. For instance, the direct *ab initio* approach usually provides us with the structural phase of local energy minimum (in contrast to the most stable phase of global energy minimum), which is exacerbated by the 0 K assumption adopted. The application of this approach often requires the comparison of many different phases that may not be able to cover all phases. To address this problem, here we adopt the first-principles based effective Hamiltonian approach and Monte-Carlo (MC) simulations, which were developed exactly to address such challenges. To use this approach, it is necessary to compute tens of coefficients appearing in the effective Hamiltonian using direct *ab initio* computation before carrying out the MC simulations.

The effective Hamiltonian used here was originally developed in Ref. [31], which incorporates the coupled dynamics of the soft mode, strain, and dipole. Its internal energy is given by

$$E = E^{\text{FE}}(\{\mathbf{u}_i\}, \{\mathbf{v}_i\}, \eta_H),$$

where \mathbf{u}_i is the local soft-mode in unit cell i , and is proportional to the local electric dipole moment in that cell when multiplied by Born effective charge. We note that \mathbf{u}_i here is located on the A-site (where Sn stays), and represents the collective motion of Sn, Ti, and O atoms inside one unit cell. The \mathbf{v}_i are Sn-centered local displacements related to the inhomogeneous strain inside each unit cell. η_H is the homogeneous strain tensor. The energy terms and associated parameters can be found in Ref. [32]. In this work, we extended the effective Hamiltonian and expanded the local energy term to 8th order (similar to Ref. [33]) in order to describe the internal energy more precisely [34]. In addition, the antiferro-distortive (AFD) oxygen octahedron tilting is also considered with the energy term becoming [35]

$$E = E^{\text{AFD}}(\{\boldsymbol{\omega}_i\}, \{\mathbf{u}_i\}, \{\mathbf{v}_i\}, \eta_H),$$

where the new variable $\boldsymbol{\omega}_i$ represents the oxygen tilting on the unit cell i , which centres on the B-site atom (i.e., Ti). The energy term E^{AFD} also includes the couplings between AFD, and all the other dynamical variables. The associated parameters in E^{AFD} are obtained in a similarly way as in Ref. [32,36]. The effective Hamiltonian approach is a well established methodology that has been developed since 1994 [31,37] and similar to direct *ab initio* methods, it has been used in many investigations, e.g., to predict new structural phases of perovskites [38,39]. The most appealing features of this approach are (i) It can often lead us to the most stable structural phase of global energy minimum; (ii) It can produce finite temperature properties, which explains why we adopt this approach in this work.

With the effective Hamiltonian, we perform MC simulations on a $12 \times 12 \times 12$ supercell, containing 8640 atoms. The system is set to meet the periodic boundary condition along the (pseudo) x, y, z directions and subject to various epitaxial strains. In each simulation at a given epitaxial misfit strain s , we gradually cool down the system from 2500 K to 5 K. For each temperature, we carry out 160,000 MC steps to obtain averaged physical quantities – most importantly – the supercell average of local mode, which can be used to determine the symmetry of the system and the approximate positions of each atom in it.

We have also performed direct *ab initio* computation to corroborate MC simulation results. For this purpose, the open source ABINIT software package [40] is used along with the local density approximation (LDA) [41] and the projector-augmented-wave (PAW) method [42]. We use the pseudo-potentials implemented in the GBRV package [43], and the Sn $4d\ 5s\ 5p$, Ti $3s\ 3p\ 4s\ 3d$, and O $2s\ 2p$ orbitals are treated as valence orbitals. For convergence, we have chosen the cut-off energy (`ecut`) to be 25 Hartree (1 Hartree = 27.211 eV) for plane wave expansion, and fine grid the cut-off energy (`pawcutdg`) is selected to be 50 Hartree. In addition, k -point sampling of $6 \times 6 \times 6$ Monkhorst-Pack grid [44] was used. The atomic coordinates are relaxed until all atomic-force components are smaller than 10^{-5} Ha/Bohr, and the cell size and shape are varied until all stress components are below 10^{-7} Hartree/Bohr³.

Both the MC simulations and the direct *ab initio* computations deal with the strained bulks (in contrast to ultrathin two-dimensional films) given the periodic boundary condition used. However, many properties of the strained films (as long as they are *not* just a few atomic layers thick) can be inferred from such calculations. Comparing to our previous work [32], the present investigation develops in three directions: (i) We now include the new degree of freedom, i.e., oxygen octahedron tilting (often called antiferrodistortive rotations, AFD), which is ignored in the previous work [32]. (ii) To this end, we computed many new essential parameters for the effective Hamiltonian. While the current work build on the previous one, it has substantially extended the effort to fully simulate SnTiO₃. (iii) Here we consider the effects of epitaxial strain and show that SnTiO₃ has a rather complex phase diagram, containing interesting phase boundaries and triple points.

3. Results

In order to obtain the phase diagram, we have performed MC simulations for misfit strain between $s = 0$ and $s = 2\%$ with a step size of $\Delta s = 0.125\%$. For each misfit strain s , the system is gradually cooled down from ~ 2500 K to 5 K and its evolution with temperature is observed. The simulation results are then summarized to form the phase diagram.

3.1. Phase transition and phase diagram

We first obtain the supercell averaged local mode versus temperature of SnTiO₃ under various tensile epitaxial strains, which is expected to stabilize SnTiO₃ [19]. Such information enables us to find the evolution of structural phases with respect to temperature and epitaxial strain, and more importantly, the phase transition temperatures of the system. Figure 1 shows the results with misfit strain $s = 0.375\%$ and $s = 1\%$. Note that we have relaxed the cubic phase ($Pm\bar{3}m$) SnTiO₃ using ABINIT (with settings specified in Sec. 2.) to obtain the lattice parameter $a = 7.312$ Bohr, which is used as the reference value for specifying the misfit strain.

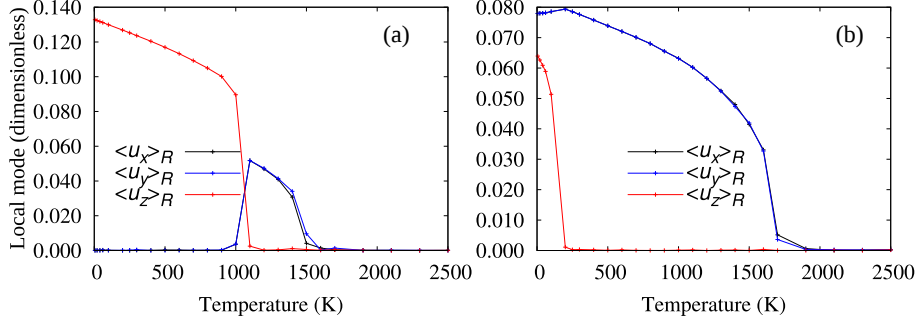


Figure 1: Local mode versus temperature at two given strain misfit, $s = 0.375\%$ (Left panel) and $s = 1\%$ (Right panel).

For the smaller epitaxial strain $s = 0.375\%$, the system adopts $P4mm$ phase for temperature $T \lesssim 1000$ K, ($P_x = P_y = 0, P_z > 0$), as the temperature increases it undergoes a phase transition to become the $Amm2$ phase ($P_x = P_y > 0, P_z = 0$), and eventually the cubic phase for $T \gtrsim 1500$ K. The whole process is somewhat similar to that of BaTiO_3 and $(\text{Na}_{0.5}\text{K}_{0.5})\text{NbO}_3$, where several structural phases are involved in phase transitions. Here, however, a rather drastic change happens at around 1000 K as the polarization rotates from out-of-plane to the in-plane configuration. For the larger epitaxial strain ($s = 1\%$), there are also two phase transitions. At low temperature ($T \lesssim 197$ K), it adopts the Cm ($P_x = P_y > 0, P_z > 0$) phase, which changes to the $Amm2$ phase as the temperature increases, and finally become paraelectric at $T \simeq 1750$ K. This phase transition temperature is high comparing to other typical ferroelectric materials, e.g., PbTiO_3 (763 K) and BiFeO_3 (1100 K) [45]. The reason is likely due to the strong dipole-dipole interaction inside SnTiO_3 , noting that the spontaneous polarization of SnTiO_3 (1.32 C/m^2) [32] is even larger than the strained BiFeO_3 (1.30 C/m^2) [46].

It is worth noting that no correlated AFD was observed for the epitaxial strains investigated here, consistent with previous known results [19] (also see Sec. 4). Figure 1 indicates that four phases (paraelectric $Pm\bar{3}m$, orthorhombic $Amm2$, tetragonal $P4mm$, and monoclinic Cm) can all exist in SnTiO_3 at proper temperature and epitaxial strain. Without strain constraint or at tiny strain ($s < 0.5\%$, see Fig. 2), the system adopts the $P4mm$ phase ($P_z > 0, P_{x,y} = 0$) at low temperature, and only has one phase transition ($P4mm$ to paraelectric) as temperature increases. Interestingly, Figure 1(b) shows a region ($T \leq 200$ K) that corresponds to the M_B phase (belong to space group Cm) [34,47], and for smaller s (e.g., at $s = 0.75\%$), we have observed that $P_z > P_x = P_y$, which is also Cm , but corresponds to the M_A phase [47]. Moreover, in Figure 1(a), both the M_A and M_B phases exist between the T ($P4mm$) and O ($Amm2$) phases. The phase transition sequence resembles the local structure evolution of $\text{Pb}(\text{Ti}_{1-x}\text{Zr}_x)\text{O}_3$ with increasing x [48]. Such monoclinic region has been shown to play critical role in high-performance piezoelectric materials [49].

We now turn to the phase diagram of SnTiO_3 with respect to temperature and epitaxial strain. First, for all the investigated misfit strains (up to 2%), Fig. 2 shows that SnTiO_3 undergoes a paraelectric to ferroelectric phase transition at rather high temperature ($T_C > 1400$ K). The high T_C is likely due to the large intrinsic spontaneous polarization discussed previously [32]. Second, T_C initially decreases with s , reaching a minimum, and then increases again [50], the lowest point corresponds to a triple point separating the paraelectric phase and the other two ferroelectric phases (tetragonal $P4mm$ and orthorhombic $Amm2$), similar to what happens

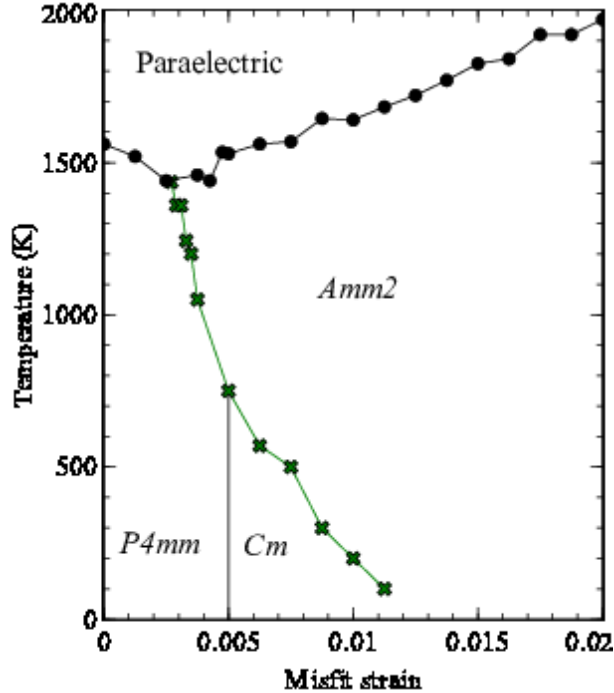


Figure 2: Phase diagram of epitaxially strained SnTiO₃.

in ultrathin PbTiO₃ films [15]. We note that the existence of the *Cm* phase is consistent with results obtained in Ref. [19]. The abrupt transition from the *P4mm* to the *Cm* phase (with respect to the misfit strain) happens in a slender region ($< 0.125\%$) represented by a straight line in Fig. 2 due to the limit of Δs used in simulations.

The first triple point in Fig. 2, where one paraelectric cubic phase and two ferroelectric phases converge, contains potential giant piezoelectric effects. For instance, such triple point was found and exploited in binary compounds including (Ba_{0.7},Ca_{0.3})TiO₃-Ba(Zr_{0.2},Ti_{0.8})O₃ (BCZT) [4], Ba(Sn_{0.12},Ti_{0.88})O₃-*x*(Ba_{0.7},Ca_{0.3})O₃ [51], and other BaTiO₃-derived systems [52]. More importantly, the three ferroelectric phases (*P4mm*, *Amm2*, and *Cm*) converge to a second triple point. There are three boundaries around this point. The boundary at $s = 0.5\%$ separates the *P4mm* and the *Cm* phase, resembling the MPB seen in Pb(Zr_{1-*x*},Ti_{*x*})O₃, in which two different structural phases exist with a buffer region at $x \simeq 0.48$. In Pb(Zr_{1-*x*},Ti_{*x*})O₃ the monoclinic phase serves as a bridge between the higher symmetry tetragonal phase (with [001] polarization) and the rhombohedral phases (with [111] polarization) [35]. In this connecting phase, the polarization can align anywhere on the {110} mirror plane between the pseudocubic [111] and [001] directions, giving rise to the high piezoelectric response [35,53,54].

Here in SnTiO₃, the pronounced existence of the *Cm* phase and the second triple point, which bridges the tetragonal phase (with [001] polarization) and the orthorhombic phase (with [110] polarization), may also enable high performance, following the pattern of the universal phase diagram discussed in Ref. [53,54]. The reason is similar to that of Pb(Zr_{1-*x*},Ti_{*x*})O₃: in this region, polarization anisotropy nearly vanishes and thus polarization rotations are easy [47]. Many alkaline niobate perovskites show a polymorphic phase transition [55] between the tetragonal phase and the orthorhombic phase, similar to what happens in Fig. 2. The polymorphic behaviour can also lead to high piezoelectricity due to the instability with respect to polarization rotation [56]. However, the temperature stability of their piezoelectric properties for alkaline niobate perovskites is not as good

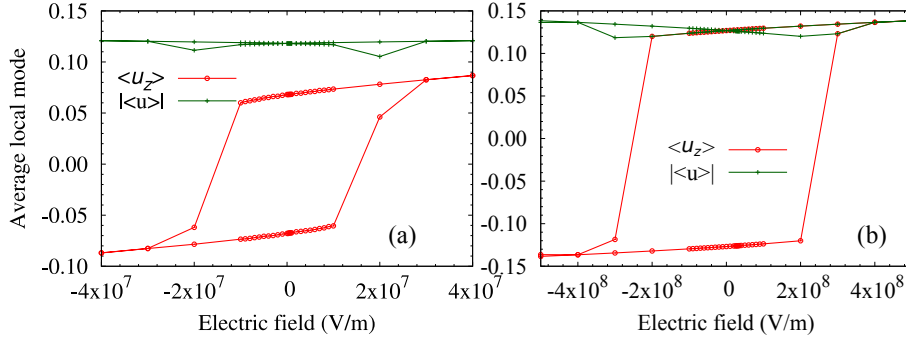


Figure 3: Hysteresis loop of SnTiO₃ at $s = 0.75\%$ (a) and $s = 0\%$ (b) at 300 K. The electric field is applied along the z -axis.

as Pb(Zr_{1-x}Ti_x)O₃. In addition, the large anisotropy along the whole polymorphic boundary line leads to a larger energy barrier between the two polarization states (tetragonal and orthorhombic), preventing possible polarization rotations because the phase coexistence results from the diffusive tetragonal to orthorhombic phase transformation. [4] In SnTiO₃, unlike the polymorphic phase transition, the Cm phase is associated with a triple point, where a low energy barrier between two ferroelectric phases ($P4mm$ and $Amm2$) may exist that facilitates the polarization rotation and lattice distortion, leading to high performance. Unfortunately, this triple point is not at room temperature for pure SnTiO₃ (which is at ~ 750 K as shown in Fig. 2), and may need to be tuned (e.g. by doping). For instance, following the lessons from BCZT, it may be possible to use Pb to substitute Sn and/or Zr to substitute Ti. In this way, SnTiO₃ can be taken as the matrix material for designing high performance piezoelectric materials.

To show that the polarization in the Cm phase can easily rotate, we also obtained the hysteresis loop at different epitaxial strains. As Fig. 3 shows, the Cm phase has a strong effect on the hysteresis loop of SnTiO₃. When the Cm phase exists [Fig. 3(a)] at $s = 0.75\%$, the coercive field is $\sim 1.6 \times 10^7$ V/m, reduced by a factor of 10 compared to the result obtained when $s = 0\%$ ($> 2 \times 10^8$ V/m, see Fig. 3(b)). In analogous to magnetic materials, by applying a proper strain (e.g., 0.75%), SnTiO₃ becomes “soft” ferroelectrics. Interestingly, in the whole process, the magnitude of the polarization \mathbf{P} is approximately a constant [dark green line in Fig. 3], making the whole process a rotation as well as switching of polarization (albeit a sudden rotation), consistent with previous computations [29,30].

3.2. Direct *ab initio* computation

To corroborate results obtained from effective-Hamiltonian-based computations, we also obtained numerical results from direct *ab initio* computation. Figure 4(a) shows the energy versus strain for the $P4mm$, $Amm2$, and Cm phases. These phases all appear in the phase diagram of SnTiO₃ (Fig. 2). For a large range of epitaxial strain, the Cm phase has the lowest energy. At $s = 1\%$, the energy of the Cm phase is approximately 29.4 meV lower than that of $P4mm$ or $Amm2$. Such results indicate that the Cm phase can be the ground state for a restricted range of strain, which supports our effective Hamiltonian results. The Cm phase appears around $s = 0.5\%$ is likely because at this point the three phases (Cm , $P4mm$, and $Amm2$) have similar energies, and macroscopically the average of $P4mm$ and $Amm2$ also give rise to the Cm phase. On the other hand, when

$s > 1\%$, $P4mm$ is no longer an option as its energy becomes much higher than the other two. As the energy difference between $Amm2$ and Cm continue to be smaller with the misfit strain, the Cm phase can only exist at low temperatures, and eventually disappears. The Cm phase rarely appear in pure perovskites, whether it is epitaxially strained or not, and SnTiO_3 seems to be an important exception. Figure 4(b) plots the polarization versus the misfit strain for the Cm phase, which is similar to the results obtained in Ref. [19], showing that P_z increases while $P_{x,y}$ decreases with increasing epitaxial strain. We finally note that, despite many attempts, no structural phases involving AFD tilting were found to be the ground state. For $0\% < s < 5\%$, structural phases without AFD are consistently more stable in terms of energy.

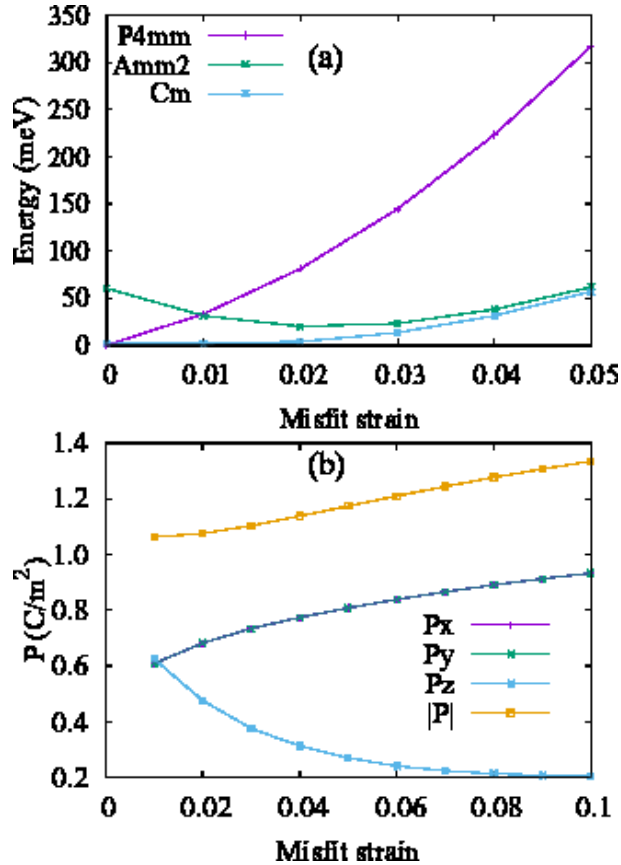


Figure 4: (a) Energy and polarization versus strain for three different phases $Amm2$, $P4mm$, and Cm . At $s = 0\%$; (b) The polarization ($P_x = P_y$ and P_z) versus strain for the Cm phase.

4. Discussion

In Sec. 3. we have shown that SnTiO_3 has $P4mm$, $Amm2$ and Cm phases under different conditions. However, it is hard to prove that SnTiO_3 can only has these three phases for the misfit strain we have investigated. This point is further discussed below in Sec. 4.1. Moreover, we will compare the MC results to direct *ab initio* results and focus on the Cm phase in Sec. 4.2.

4.1. Seeking new phases

Phonon calculations have shown that for SnTiO₃ the AFD-related modes are also unstable [19]. Considering this fact, it is rather surprising that the MC simulation results are not able to identify new phases involving oxygen octahedron tilting, which is a pity and an important lesson.

We had intentionally played with the coefficients in the effective Hamiltonian and performed additional MC simulations in order to suggest new phases involving AFD. The simulation results indeed generated a few AFD-related candidates (e.g., the *Ima2*, *Imma*, and *I4cm* phases). However, direct *ab initio* calculations do not validate them as energy ground states, consistent with the fact that Parker *et al* did not propose any AFD related phases although their calculations have shown strong AFD instability [19]. Therefore, our results strongly suggest that SnTiO₃ may not have AFD-related phases as ground state for the misfit strain of $s < 5\%$.

The fact that AFD-related phases do not appear is most likely due to the strong competition from the polar local mode, which is responsible for the polarization in SnTiO₃. For ferroelectric materials, AFD is usually adverse to the development of polarization. One term in the effective Hamiltonian specifically represents such an effect, which is $D\omega^2\mathbf{u}^2$ [57], where the sign of the coupling coefficient (D) will determine how strong the competition (or in rare cases the cooperation) between the local mode \mathbf{u} (related to polarization) and ω (related to AFD). In SnTiO₃, apparently the ferroelectric local mode (which are responsible for the *P4mm*, *Amm2*, and *Cm* phases) dominate the system.

4.2. The *Cm* phase

The results from *ab initio* computations in Fig. 4 show that the *Cm* phase has the lowest energy beyond $s = 0$ among the *P4mm*, *Cm* and *Amm2* phases. On the other hand, the phase diagram obtained from MC simulations shows that SnTiO₃ exhibits the *Cm* phase in a much smaller misfit strain range. The most likely reason of this discrepancy is that the lone pair on Sn²⁺ can cause the extra out-of-plane polarization that is not well accounted for in the effective Hamiltonian, where the polarization is closely related to the Γ -point (of the cubic phase) unstable polar mode [31].

For SnTiO₃ that mode is $u_{x,y,z} = (\xi_{\text{Sn}}, \xi_{\text{Ti}}, \xi_{\text{O}_{\text{all}}}, \xi_{\text{O}_{\perp}}, \xi_{\text{O}_{\perp}}) = (0.534, 0.169, -0.411, -0.508, -0.508)$ (normalized), which approximately represents the ion displacements in SnTiO₃ and specifies how spontaneous polarization develops. However, some anomaly happens for SnTiO₃ as can be seen from the direct *ab initio* computation. For instance, at $s = 1\%$, along the z direction the ion displacements are $u'_z = (0.847, 0.352, -0.049, -0.27, -0.27)$ while along the x, y directions, $u'_{x,y} = (0.781, 0.259, -0.150, -0.387, -0.387)$. It is important to note that u' has a much larger weight on Sn²⁺, which is not reflected in u . In fact, this is a known issue during the development of the effective Hamiltonian approach as discussed in Ref. [37] where it was pointed out that for KNbO₃ and PbTiO₃ there is large difference between the experimental and theoretical local modes. Here, SnTiO₃ has the same problem while the difference between PbTiO₃ and SnTiO₃ is discussed in detail in Ref. [58]. In principle, for SnTiO₃ it is possible to tune the values of u (or adding an extra polar mode) in the effective Hamiltonian to alleviate or fix this issue. But such a move will involve many more cumbersome calculations of coupling coefficients, making the approach more complicated. This issue again shows the complexity of SnTiO₃ despite its simple composition.

5. Conclusion

Using effective Hamiltonian based Monte Carlo simulations, we have investigated epitaxially strained SnTiO₃, found their structural phases at finite temperatures, and obtained its phase diagram with respect to temperature and misfit strain. The phase diagram of SnTiO₃ turns out to be rather complicated, containing two triple points and boundaries that separate ferroelectric phases. Such special features provide unique opportunities to design novel high-performance ferroelectric materials containing SnTiO₃, in which the rarely seen *Cm* phase can exist. In addition, while phonon calculation had shown that AFD related modes are unstable [19], no AFD-related structural phases were found in our simulations, which is likely due to the strong competition from unstable polar modes.

References

- [1] Xu R J, Liu S, Grinberg I, Karthik J, Damodaran A R, Rappe A M and Martion L W 2015 *Nature Mater.* **14** 79
- [2] Jaffe B, Cook W R and Jaffe H 1971 *Piezoelectric Ceramics* (London: Academic)
- [3] Saito Y, Takao H, Tani T, Nonoyama T, Takatori K, Homma T, Nagaya T and Nakamura M 2004 *Nature* **432** 84
- [4] Liu W F and Ren X B 2009 *Phys. Rev. Lett.* **103** 257602
- [5] Jaffe B, Roth R S and Marzullo S 1954 *J. Appl. Phys.* **25** 809
- [6] Zeng Y, Bokov A A, Wang D, Xiang F, and Hong W, 2018 *Ceram. Inter.* **44** 17548
- [7] Wessels B W 2007 *Ann. Rev. Mater. Res.* **37** 659
- [8] Ramesh R and Spaldin N A 2007 *Nat. Mater.* **6** 21
- [9] Hwang H Y, Iwasa Y, Kawasaki M, Keimer B, Nagaosa N and Tokura Y 2012 *Nature Mater.* **11** 103
- [10] Yamada H, Ogawa Y, Ishii Y, Sato H, Kawasaki M, Akoh H and Tokura Y 2004 *Science* **305** 646
- [11] Ohtomo A and Hwang H Y 2004 *Nature* **427** 423
- [12] Spaldin N A and Fiebig M 2005 *Science* **309** 391
- [13] Wang L, Ju S, You L, Qi Y J, Guo Y W, Ren P, Zhou Y and Wang J L 2015 *Sci. Rep.* **5** 18707
- [14] He F Z, Wells B O, Ban Z G, Alpay S P, Grenier S, Shapiro S M, Si W D, Clark A and Xi X X 2004 *Phys. Rev. B.* **70** 235405
- [15] Jiang Z J, Zhang R Z, Wang D W, Sichuga D, Jia C L and Bellaiche L 2014 *Phys. Rev. B* **89** 214113
- [16] Wu J, Xiao D and Zhu J 2015 *Chem. Rev.* **115** 2559
- [17] Armiento R, Kozinsky B, Fornari M and ceder G 2011 *Phys. Rev. B* **84** 014103; Matar S, Baraille I and Subramanian M 2009 *Chem. Phys.* **355** 43

- [18] Lebedev A I 2009 *Phys. Solid State* **51** 362
- [19] Parker W D, Rondinelli J M and Nakhmanson S M 2011 *Phys. Rev. B* **84** 245126
- [20] Xie Y H, Yin S, Hashimoto T, Kimura H and Sato T 2009 *J. Mater. Sci.* **44** 4834
- [21] Ren P R, Liu Z C, Wang Q, Peng B L, Ke S M, Fan H Q and Zhao G Y 2017 *Sci. Rep.* **7** 6693
- [22] Bennett J W, Grinberg I, Davies P K and Rappe A M 2011 *Phys. Rev. B* **83** 144112
- [23] Suzuki S, Honda A, Iwaji N, Higai S, Ando A, Takagi H, Kasatani H and Deguchi K 2012 *Phys. Rev. B* **86** 060102
- [24] Laurita G, Page K, Suzuki S and Seshadri R 2015 *Phys. Rev. B* **92** 214109
- [25] Agarwal R, et al, 2018 *Phys. Rev. B* **97** 054109
- [26] Taib M F M, Yaakob M K, Hassan O H and Yahya M Z 2013 *Integr. Ferroelectr.* **142** 119
- [27] Taib M F M, Yaakob M K, Badrudin F W, Kudin T I T, Hassan O H and Yahya M Z A 2014 *Integr. Ferroelectr.* **459** 134
- [28] Uratani Y, Shishidou T and Oguchi T 2008 *Jpn. J. Appl. Phys.* **47** 7735
- [29] Zhang R Z, Wang D W, Li F, Ye H J, Wei X Y and Xu Z 2013 *Appl. Phys. Lett.* **103** 062905
- [30] Zhang R Z, Wang D W, Zhu X H, Ye H J, Wei X Y and Xu Z 2014 *J. Appl. Phys.* **116** 174101
- [31] Zhong W, Vanderbilt D and Rabe K M 1994 *Phys. Rev. Lett.* **73** 1861; 1995 *Phys. Rev. B* **52** 6301
- [32] H J Ye, Wang D W, Jiang Z J, Cheng S and Wei X Y 2016 *Acta Phys. Sin.* **65** 237101
- [33] Nishimatsu T, Iwamoto M, Kawazoe Y, and Waghmare U V 2010 *Phys. Rev. B* **82** 134106
- [34] Vanderbilt D and Cohen M H 2001, *Phys. Rev. B* **63** 094108
- [35] Kornev I A, Bellaiche L, Janolin P E, Dkhil B and Suard E 2006 *Phys. Rev. Lett.* **97** 157601
- [36] Ye H J, Zhang R Z, Wang D W, Cui Y, Wei J, Wang C L, Xu Z, Qu S B and Wei X Y 2013 *Int. J. Mod. Phys. B* **27** 1350144
- [37] King-Smith R D and Vanderbilt D 1994 *Phys. Rev. B* **49** 5828
- [38] Jiang Z J, Xu B, Li F, Wang D, and Jia C.-L. 2015 *Phys. Rev. B* **91** 014105
- [39] Al-Barakaty A, Prosandeev S, Wang D, Dkhil B, Bellaiche L 2015 *Phys. Rev. B* **91** 214117
- [40] Gonze X, Beuken J M, Caracas R, Detraux F, Fuchs M, Rignanese G M, Sindic L, Verstraete M, Zerah G, Jollet F, Torrent M, Roy A, Mikami M, Ghosez P, Raty J Y and Allan D C 2002 *Comp. Mat. Sci.* **25** 478
- [41] Perdew J P and Wang Y 1992 *Phys. Rev. B* **45** 13244
- [42] Blochl P E 1994 *Phys. Rev. B* **50** 17953

- [43] Garrity K F, Bennett J W, Rabe K M and Vanderbilt D 2014 *Comput. Mater. Sci.* **81** 446
- [44] Monkhorst H J and Pack J D 1976 *Phys. Rev. B* **13** 5188
- [45] Liu K, Fan H Q, Ren P R and Yang C 2010 *J. Alloy. Comp.* **509** 1901
- [46] Zhang J X, et al, 2011 *Phys. Rev. Lett.* **107** 147602
- [47] Zhang N, Yokota H, Glazer A M, Ren Z, Keen D A, Keeble D S, Thomas P A and Ye Z G 2014 *Nat. Commun.* **5** 5231
- [48] Lu X, Zheng L, Li H and Cao W 2015 *J. Appl. Phys.* **117** 134101
- [49] Liu H, Chen J, Fan L, Ren Y, Pan Z, Lalitha K. V., Rdel J and Xing X, 2017 *Phys. Rev. Lett.* **119**, 017601
- [50] Schlom D G, Chen L Q, Eom C B, Rabe K M, Streiffer S K and Triscone J M 2007 *Annu. Rev. Mater. Res.* **37** 589
- [51] Xue D Z, Zhou Y M, Bao H X, Gao J H, Zhou C and Ren X B 2011 *Appl. Phys. Lett.* **99** 122901
- [52] Liu L J, Zheng S Y, Huang Y M, Shi D P, Wu S S, Fang L, Hu C Z and Elouadi B 2012 *J. Phys. D: Appl. Phys.* **45** 295403
- [53] Guo R, Cross L E, Park S E, Noheda B, Cox D E and Shirane G 2000 *Phys. Rev. Lett.* **84** 5423
- [54] Cox D E, Noheda B, Shirane G, Uesu Y, Fujishiro K and Yamada Y 2001 *Appl. Phys. Lett.* **79** 400
- [55] Liu L J, Huang Y M, Li Y H, Fang L, Dammak H, Fan H Q and Thi M P 2012 *Mater. Lett.* **68** 300
- [56] Wada S, Suzuki S, Noma T, Suzuki T, Osada M, Kakihana M, Park S E, Cross L E and Shrout T R 1999 *Jpn. J. Appl. Phys.* **38** 5505
- [57] Wang D W, et al, 2011 *Phys. Rev. Lett.* **107** 175502
- [58] Pitike K C, Parker W D, Louis L, and Nakhmanson S M, 2015 *Phys. Rev. B* **91** 035112